Nanoscale

PAPER

View Article Online
View Journal | View Issue

Check for updates

Cite this: *Nanoscale*, 2024, **16**, 20089

Modulating the photodynamic modality of Au_{22} nanoclusters through surface conjugation of arginine for promoted healing of bacteria-infected wounds†

Xinyue Dou,*[a] Sariah Saalah,[a] Chel-Ken Chiam,[a] Jianping Xie *[b] and Coswald Stephen Sipaut*[a]

Developing novel antibacterial agents without drug resistance is highly desired but challenging. In this study, an Au nanocluster (NC)-based photodynamic antibacterial agent with aggregation-induced emission (AIE) has been designed to promote the healing of bacteria-infected wounds by conjugating arginine (Arg) on the surface of Au_{22} NCs. The conjugation of Arg not only endows the NCs with enhanced visible light absorption, increased photoluminescence (PL) intensity, and prolonged PL lifetime, but it also enables switching the photodynamic production mode of reactive oxygen species (ROS) and extra production of reactive nitrogen species (RNS). These enhancements allow the Arg-Au_{22} NCs to combine ROS/RNS-mediated antibacterial action with the enhanced inherent antibacterial properties of Au NCs, resulting in outstanding antibacterial efficacy against both Gram-negative and Gram-positive bacteria. *In vivo* experiments demonstrate the effective treatment of bacteria-infected wounds by the Arg-Au_{22} NCs, leading to the photodynamic eradication of bacterial infections and reduced inflammation in the wound area without causing systemic harm or impairing blood and liver functions. This study introduces a novel approach to designing metal NC-based photodynamic antibacterials with multiple antibacterial actions, contributing to deeper understanding of ROS/RNS-mediated antibacterial mechanisms, and future utilization of metal NCs in antibacterial therapies.

Received 9th August 2024,
Accepted 26th September 2024

DOI: 10.1039/d4nr03278k

rsc.li/nanoscale

Published on 11 October 2024. Downloaded on 2/23/2026 2:18:25 PM.

1. Introduction

Developing high-efficacy and broad-spectrum antibacterials is a continuous goal for researchers due to the pressing requirements of public health, especially given that conventional antibiotics suffer from severe drug resistance and narrow-spectrum antibacterial behavior.[1] In recent years, metal nanomaterials, as a category of inorganic antibacterial agents, have attracted significant interest due to their widespread applicability and broad-spectrum antibacterial properties.[1–7] Notably, ultrasmall coinage metal nanoclusters (*e.g.*, Ag, Au, and Cu NCs)[8–21] represent a novel class of antibacterials that have shown intrinsic bactericidal activity in combating bacteria.[4,6,22–27] Despite their efficacy, the practical use of these antibacterial agents is often hindered by their limited duration of effectiveness attributed to the consumption of NCs *via* metal ion release or cell endocytosis.[28] To address this limited effectiveness, researchers have designed Au NCs with aggregation-induced emission (AIE[29]) as photodynamic antibacterial agents.[28,30,31] AIE-type metal NCs uniquely generate reactive oxygen species (ROS) under light exposure, efficiently deactivating bacteria. This trait presents an innovative strategy for reliable and enduring photodynamic bacterial inactivation as an alternative to traditional oxidation methods.[2,28] In comparison with Ag and Cu NCs, Au NCs were found to exhibit superior biosafety,[32] driving their broader acceptance in addressing bacterial infections *in vivo*. However, the development of Au NC-based photodynamic antibacterial agents is currently in its early stages.[28,31,33] Further research is urgently required to explore the *in vivo* applications, design principles, and photodynamic modulation mechanisms of Au NCs.

At present, conventional Au NC-based antibacterials face several design limitations: (1) despite the development of several Au NC-based photodynamic antibacterials,[28,31,33] the limited research on regulating their photodynamic properties

[a]*Chemical Engineering Programme, Faculty of Engineering, Universiti Malaysia Sabah, Kota Kinabalu 88400, Sabah, Malaysia. E-mail: jojoba2021@126.com, css@ums.edu.my*
[b]*Department of Chemical and Biomolecular Engineering, National University of Singapore, 4 Engineering Drive 4, Singapore, 117585, Singapore. E-mail: chexiej@nus.edu.sg*

† Electronic supplementary information (ESI) available. See DOI: https://doi.org/10.1039/d4nr03278k

Published on 11 October 2024. Downloaded on 2/23/2026 2:18:25 PM.

has hindered the understanding of their antibacterial mechanism and impeded the development of more efficient NC-based photodynamic antibacterials; (2) current research primarily concentrates on the photodynamic generation of ROS for bacteria killing, while overlooking the investigation into producing reactive nitrogen species (RNS) with enhanced toxicity against bacteria;[34,35] and (3) while Au NC-based photodynamic agents show promise for *in vitro* broad-spectrum antibacterial applications,[28,31,33] their potential *in vivo* antibacterial effects remain understudied.[36] Therefore, it is urgently demanded that Au NCs are rationally designed to achieve the modulation in photodynamic production of ROS and concurrent RNS production. This novel approach would enable the synergistic coupling of ROS and RNS with the intrinsic antibacterial properties of Au NCs, offering a comprehensive strategy to combat bacterial infections *in vivo*, and deepening the understanding on the antibacterial mechanisms of metal NCs, which may shed light on the design of other high-performance metal NC-based photodynamic antibacterials.

Herein, we present the design of an Au NC-based photodynamic antibacterial agent for enhanced healing of bacteria-infected wounds, which is achieved through conjugating AIE-featured Au_{22} NCs with arginine (Arg) molecules *via* simple 1-(3-dimethylaminopropyl)-3-ethylcarbodiimide hydrochloride (EDC)/*N*-hydroxysuccinimide (NHS) crosslinking (Scheme 1). The Arg conjugation with the Au_{22} NCs provides several key advantages: (1) it enhances visible light absorption, increases the photoluminescence (PL) intensity, and prolongs PL lifetimes, thereby improving the photodynamic antibacterial performance; (2) it facilitates the transition in the production of reactive oxygen species (ROS) from the superoxide anion ($^{\bullet}O_2^-$) to H_2O_2 and hydroxyl radicals ($^{\bullet}OH$) with stronger oxidative bactericidal activity,[37] while also enabling the extra production of RNS and prompting the intrinsic antibacterial activity of Au NCs because the alteration of surface charges from negative to neutral/positive enhances their interaction with negatively charged bacteria, allowing for a synergistic combination of ROS/RNS-mediated antibacterial action and the inherent antibacterial properties of Au NCs (Scheme 1); and (3) the biocompatibility of the modified Au_{22} NCs is further improved due to the excellent biocompatible attribute of natural amino acids such as Arg. The resulting Arg-grafted Au_{22} NCs (referred to as Arg-Au_{22} NCs) exhibit outstanding photodynamic antibacterial efficacy against both Gram-negative and Gram-positive bacteria. The underlying photodynamic antibacterial mechanism was also comprehensively studied. *In vivo* experiments demonstrated the efficient treatment of bacteria-infected wounds by the Arg-Au_{22} NCs, leading to the eradication of bacterial infections and reduction of inflammation in the skin wound area. The Arg-Au_{22} NCs showed low cytotoxicity and high biosafety, demonstrating no harm to major organs and leaving blood biochemistry and liver functions unaffected. This study is significant as it not only introduces a novel approach in designing Au NC-based photodynamic antibacterials by combining three antibacterial actions into one for *in vivo* therapeutic applications, but also advances our understanding of ROS/RNS-mediated antibacterial mechanisms, paving the way for the future utilization of metal NCs in antibacterial therapies.

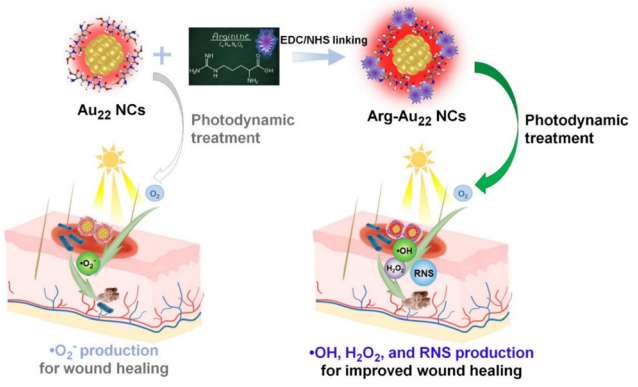

Scheme 1 Schematic illustration of the conjugation of Arg with Au_{22} NCs for promoted photodynamic healing of bacteria-infected wounds primarily due to ROS/RNS-mediated antibacterial action.

2. Experimental section

2.1. Synthesis of $Au_{22}(GS)_{18}$ NCs with aggregation-induced emission (AIE)

In this study, the AIE-featured $Au_{22}(GS)_{18}$ NCs were synthesized *via* a modified $NaBH_4$ reduction method. Typically, in a 50 mL glass beaker, 46 mL of ultrapure water, 2.5 mL of $HAuCl_4$ solution (20 mM), and 1.5 mL of GSH (50 mM) were mixed together. The mixture was intensely stirred for 2 min, causing the reaction solution to change from its original light-yellow color (typical color of $HAuCl_4$ solution) to milky white. Next, a certain amount of 1 M NaOH solution was added, gradually raising the pH value to 11 and causing the solution to transition from milky white to clear. Subsequently, $NaBH_4$ (2.1 mL, 1 mM) was added, leading to a gradual color change to dark reddish brown. After stirring at 500 rpm at room temperature for 0.5 h, the pH value was adjusted to 2.5 (optimal pH at this stage) by adding a certain amount of 1 M HCl. The beaker was then sealed with a sealing film and stirred at 500 rpm for 6 h at room temperature to obtain $Au_{22}(GS)_{18}$ NCs.

2.2. Synthesis of Arg-Au_{22} NCs

In a typical synthesis, an aqueous solution of NaOH (1 M) was added to the purified solution of $Au_{22}(GS)_{18}$ NCs to adjust the pH = 8. In the meanwhile, EDC (100 μL, 575.11 mg mL^{-1}) and NHS (100 uL, 172.64 mg mL^{-1}) were added and stirred at 500 rpm for 10 min at room temperature, then Arg (100 μL, 78.39 mg mL^{-1}) was added and stirred at 500 rpm for 40 min at room temperature. After that, 21 mL of the $Au_{22}(GS)_{18}$ NC solution (pH = 8) was mixed with the Arg solution under stirring conditions. Finally, the Arg-Au_{22} NCs could be obtained after reaction for 1 h.

This journal is © The Royal Society of Chemistry 2024

Published on 11 October 2024. Downloaded on 2/23/2026 2:18:25 PM.

2.3. Photodynamic antibacterial test

Gram-negative *E. coli* and Gram-positive *S. aureus* were used as bacteria models to evaluate the photodynamic bactericidal activity of photodynamic antibacterial agents under visible light irradiation. All the glassware and solution media were sterilized in an autoclave at 121 °C for 30 min before the antibacterial test. All tests were performed under sterile conditions. The bacterial cells were cultured in LB medium in an orbital shaker at 37 °C for 18 h, subsequently centrifuged at 8000 rpm for 5 min to remove the metabolites, and finally diluted with PBS solution (0.01 M, pH 7.4) to prepare the bacterial suspension with a cell count of 10^7 CFU mL^{-1}.

In the antibacterial test, 1 mL of Arg-Au_{22} NCs (5 mM), Au_{22} NCs (5 mM), Arg (5 mM), and PBS were individually added to 4 mL of bacterial suspension. The mixture was stirred for 30 min under different conditions: (1) dark conditions; (2) visible light irradiation under air atmospheric conditions; and (3) visible light irradiation under an oxygen atmosphere. To determine the bacterial count, the final bacterial suspension was diluted 1000 times with PBS. Then, 100 μL of the diluted bacterial suspension was evenly spread on fresh LB agar plates and incubated at 37 °C for 12 h in a constant temperature incubator. The number of growing colonies on the LB agar plates was counted, and the bactericidal rate was calculated.

3. Results and discussion

3.1. Synthesis and characterization of Au_{22} NCs and Arg-Au_{22} NCs

Fig. 1a shows the molecular structure of the Arg-Au_{22} NCs. In this study, red-emitting $Au_{22}(GS)_{18}$ NCs as the luminescent and photodynamic entity of the NC-based antibacterials (here GS is GSH, which denotes the water-soluble tri-peptide glutathione)[38] were synthesized *via* a modified "NaOH-mediated $NaBH_4$ reduction" method.[39] As shown in Fig. 1b, the Au NCs show a light brown color (inset) with a shoulder peak at 520 nm in the UV-vis absorption spectrum,[38,40] preliminarily indicating the formation of monodisperse Au NCs with molecule-like optical absorptions. However, it is well-documented that large-sized Au nanoparticles (NPs) with surface plasmon resonance also have an optical absorption at ~520 nm, and we thus used transmission electron microscopy (TEM) to exclude the possible existence of large-sized Au NPs. The TEM result provides direct evidence that the as-synthesized samples are sub-3 nm NCs with an average size of ~1.86 nm (Fig. S1†). Based on this, electrospray ionization mass spectrometry (ESI-MS) was further employed to analyze the atomically precise size of the as-synthesized Au NCs (Fig. 1c), and the result discloses the high-quality synthesis of $Au_{22}(GS)_{18}$ NCs in

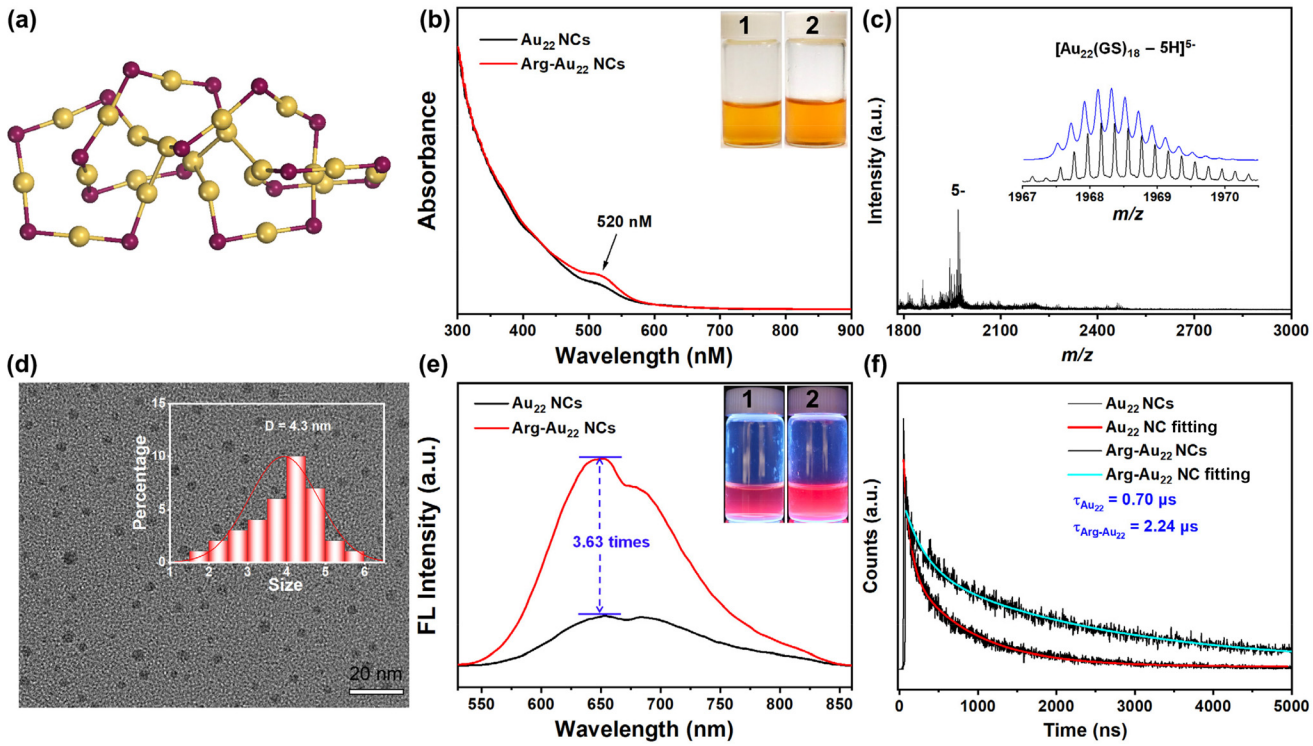

Fig. 1 (a) Schematic illustration of the structure of Arg-Au_{22} NCs (yellow balls: Au atoms; crimson balls: sulfur atoms; note that the Arg–GSH surface shell was not drawn for purposes of easy readability). (b) UV-vis absorption spectra and digital photographs (inset; taken under room illumination) of Au_{22} and Arg-Au_{22} NCs. (c) ESI-MS of Au_{22} NCs with the experimentally obtained (inset; black curve) and theoretically simulated (inset; blue curve) isotope patterns of $[Au_{22}(GS)_{18} - 5H]^{5-}$. (d) TEM image with inserted size distribution histogram of the Arg-Au_{22} NCs. (e) PL emission spectra ($\lambda_{excitation}$ = 520 nm) and digital photographs (inset; taken under UV illumination) of Au_{22} and Arg-Au_{22} NCs. (f) PL decay profiles and the corresponding fit of Au_{22} and Arg-Au_{22} NCs.

Published on 11 October 2024. Downloaded on 2/23/2026 2:18:25 PM.

which a set of peaks centered at m/z = ~1968.4 can be unambiguously determined to be $[Au_{22}(GS)_{18} - 5H]^{5-}$ with well-defined isotope patterns (inset).

In this study, Arg was selected as the functional entity of the Au_{22} NCs based on the following considerations: (1) Arg is a natural amino acid with superior biocompatibility; (2) Arg has two amino groups, one imino group, and one carboxyl group, which can modulate the surface chemistry of Au NCs and adjust the NC–bacteria interaction for possible antibacterial performance enhancement; (3) the conjugation may further rigidify the surface GSH ligands of Au NCs,[41] enhancing the PL intensity through reducing the non-radiative energy loss; and (4) Arg serves as a substrate for the endogenous synthesis of nitric oxide catalyzed by synthase *in vivo*, potentially contributing to the photodynamic production of RNS in this system.[42] Interestingly, upon conjugating with Arg through a simple EDC/NHS crosslinking process, the as-obtained Arg-Au_{22} NCs display a more noticeable shoulder absorption peak at 520 nm, while maintaining their original light brown solution color (Fig. 1b). This observation indicates that the size of the NCs remains unchanged but exhibits enhanced visible light absorption. Nevertheless, TEM analysis revealed an increase in the size of the Arg-Au_{22} NCs from 1.86 nm to 4.30 nm (Fig. 1d). The optical and size data collectively suggest the occurrence of intercluster assembly following Arg conjugation.[20,43,44] It is logical to expect such assembly given the presence of carboxyl and amino groups on both the Arg molecules and GSH ligands present on the surface of the NCs for crosslinking. Furthermore, we investigated the zeta potential (ζ) of the Au_{22} NCs both before and after conjugation with Arg. The findings revealed a shift in their surface potential at pH = 7 from negative (−12 mV) to slightly positive (+0.3 mV). This change suggests that the interaction between the Arg-Au_{22} NCs and the negatively charged bacteria (*E. coli*: −55.9 mV; *B. subtilis*: −39.4 mV) may be enhanced due to electrostatic attraction. These phenomena may enhance the photodynamic antibacterial activity of the NCs, as the increased visible light absorption, potential PL amplification caused by AIE, and strengthened NC–bacteria interaction could lead to higher local concentrations of ROS/RNS as well as bacteria near the surface of the NCs, thereby facilitating effective bacterial eradication.

We then examined the PL properties of the Au NCs. Both the Arg-Au_{22} and Au_{22} NCs exhibit identical PL emission features with two dominant peaks at 650 nm and 680 nm when excited at 520 nm, but the PL intensity of the Arg-Au_{22} NCs is 3.63 times higher than that of the Au_{22} NCs (Fig. 1e). The unchanged absorption and PL emission wavelengths indicate that the kernel size of the Au_{22} NCs remained constant following Arg conjugation. This observation is consistent with the idea that intercluster assembly, which is known to constrain ligand stretching-induced non-radiation energy loss, leads to the amplified PL intensity observed in the Arg-Au_{22} NCs.[43] Notably, both the Au_{22} and Arg-Au_{22} NCs also display intense red PL in the solid state, underscoring their AIE properties (Fig. S2†).[45] Moreover, the Arg-Au_{22} NCs exhibit slightly enhanced PL intensity at lower temperatures compared to higher ones (Fig. S3†). This is anticipated, as the energy loss due to non-radiative transitions is diminished at reduced temperature. To verify this AIE behavior, the PL lifetimes of both types of NCs (Fig. 1f) were analyzed. Our findings show that the PL lifetime of the Au_{22} NCs increases from 0.70 μs to 2.24 μs upon Arg conjugation, supporting the notion of AIE and promoting the charge carriers' separation during photodynamic applications.[46] The extended PL lifetime of the Arg-Au_{22} NCs is likely due to the electron-rich nature of the Arg moiety and the intercluster assembly, which facilitate the relaxation of ligand-to-metal charge transfer (LMCT) or ligand-to-metal–metal charge transfer (LMMCT) processes.[38,47] These results collectively highlight the visible light absorption at the molecular level, precise kernel size, favorable hydrophilicity, intense PL emission, and prolonged PL lifetime exhibited by the Arg-Au_{22} NCs, positioning them as promising candidates for applications in photodynamic antibacterial therapy.

Investigating the cytotoxicity of the Arg-Au_{22} NCs is crucial for evaluating their potential for biological applications. In this study, the 3-[4,5-dimethylthiazole-2-yl]-2,5-diphenyl tetrazolium bromide (MTT) assay was conducted using L929 mouse fibroblast cells as a model to provide quantitative data on the cytotoxicity of the Arg-Au_{22} NCs and Au_{22} NCs (Fig. S4†). Notably, the Arg-Au_{22} NCs show excellent biocompatibility with an L929 cell viability rate of >80% even at a high Au concentration of 2.5 mM. In comparison, the Au_{22} NCs exhibit an L929 cell viability of only around 32.7% at [Au] = 2.5 mM. The exceptional biocompatibility of the Arg-Au_{22} NCs can be attributed to two key factors. First, the natural amino acid Arg molecules with their intrinsic biocompatible nature contribute to the enhancement of biocompatibility. Second, upon Arg conjugation, the relatively compact ligand shell effectively shields the NCs from releasing Au^{3+} ions, further bolstering biocompatibility.

3.2. Photodynamic antimicrobial tests *in vitro*

Upon Arg conjugation, the antibacterial rates of the Au_{22} NCs against Gram-negative *Escherichia coli* (*E. coli*) and Gram-positive *Staphylococcus aureus* (*S. aureus*) showed significant improvements under visible light irradiation (60 min, 100 mW cm^{-2}), as depicted in Fig. 2. Specifically, under an air atmosphere, the photodynamic antibacterial rates of the Au_{22} NCs upon Arg conjugation ([Au] = 1 mM) increased by a noteworthy margin from ~7.5% to ~76.9% against *E. coli* and from ~38.6% to ~76.2% against *S. aureus*. Under an O_2 atmosphere, remarkable enhancements were also observed, with the antibacterial rates rising from ~70.0% to ~97.1% against *E. coli* and from ~58.8% to ~96.1% against *S. aureus*. Notably, in the absence of light exposure, the impact of Arg conjugation was still evident. The antibacterial rates of the Arg-Au_{22} NCs without light exposure showed a significant boost from ~2.1% to approximately 19.8% against *E. coli* and from ~19.0% to around 38.0% against *S. aureus*, as shown in Fig. 2a–d. Moreover, controlled experiments ruled out the possibility of direct bacteria-killing effects of both visible light (*i.e.*, the PBS

 This journal is © The Royal Society of Chemistry 2024

Published on 11 October 2024. Downloaded on 2/23/2026 2:18:25 PM.

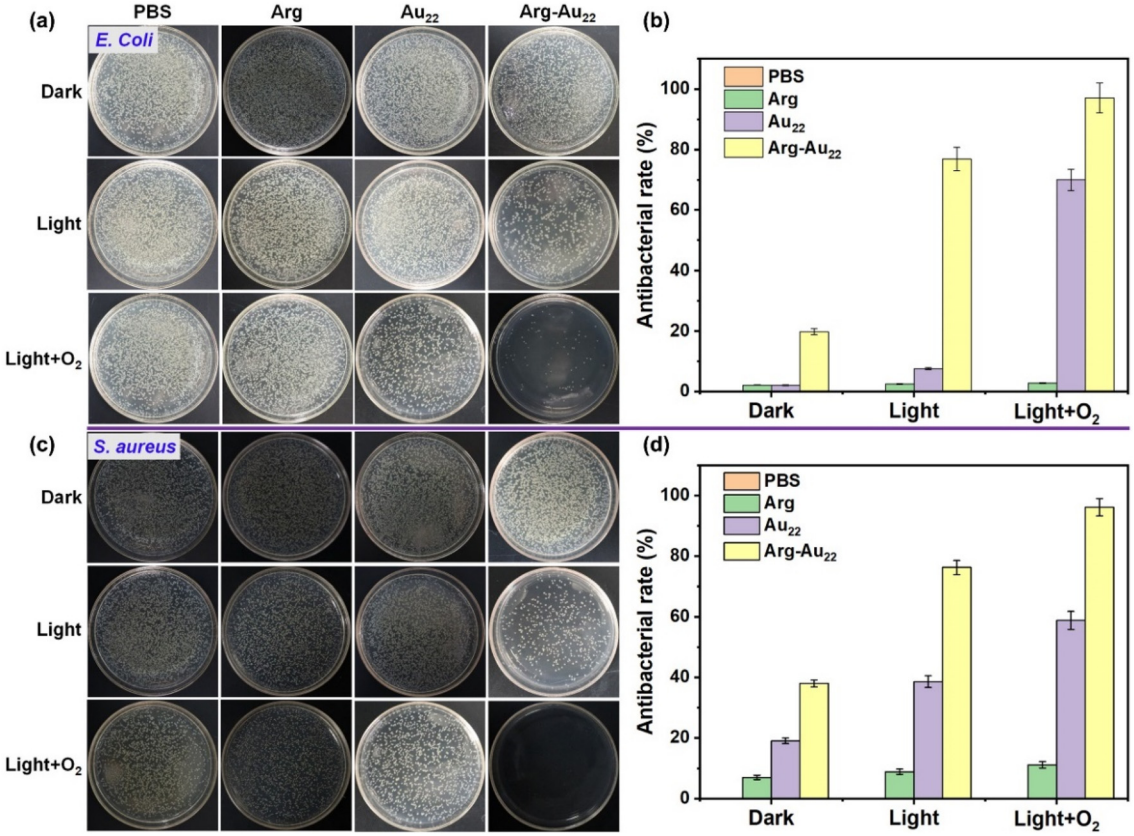

Fig. 2 Bacterial colony growth of (a) *E. coli* and (c) *S. aureus* treated with PBS, Arg, Au_{22} NCs and Arg-Au_{22} NCs under dark conditions, visible-light illumination in air, and visible-light illumination with bubbling O_2. Bactericidal activities of different samples against (b) *E. coli* and (d) *S. aureus*.

group with light irradiation) and sole Arg, as evidenced by their negligible antibacterial rates (Fig. 2). In addition to bacterial killing, the Arg-Au_{22} NCs also demonstrated the ability to effectively eradicate fungi, such as *Monilia albicans*, achieving an impressive antifungal efficacy of ~87% (Fig. S5†).

3.3. The antibacterial mechanism of Arg-Au_{22} NCs

From these observations, three key conclusions can be drawn. First, the conjugation with Arg enhances the intrinsic antibacterial activity of the Au_{22} NCs, even without light exposure. This enhancement can be attributed to the high local concentration of positively charged amino groups of Arg on the surface of the NCs that not only facilitate the interaction between the NCs and bacteria (*E. coli*: −55.9 mV; *B. subtilis*: −39.4 mV),[22] but also potentially disrupt the normal metabolism of bacterial cell membranes through electrostatic attraction with the negatively charged membrane.[1] Second, the Arg conjugation also enhances the photodynamic antibacterial efficacy of the Au_{22} NCs due to several factors, including improved visible light absorption, the presence of abundant electron-rich functional groups (such as amino and imine groups, acting as photocatalytic active centers) on the surface of the NCs, and the enhanced AIE properties of the Arg-Au_{22} NCs (*e.g.*, stronger PL intensity and prolonged charge carrier lifetime).[28,47] These factors facilitate visible light harvesting, rapid charge carrier generation/separation, and subsequent surface reactions between these NCs and bacterial cells, contributing to enhancement of photodynamic antibacterial action. Lastly, O_2 is crucial in the photodynamic antibacterial mechanism.[28] The antibacterial activity of the Arg-Au_{22} NCs significantly increases under an O_2 atmosphere compared to air, indicating a higher production of ROS that are essential for eradicating bacteria. These results confirm the successful surface modification of the AIE-functionalized Au_{22} NCs with Arg to enhance their photodynamic antibacterial properties.

Answering the question of why the Arg-Au_{22} NCs exhibit exceptional photodynamic antibacterial activities is crucial as it can advance the understanding of the photodynamic antibacterial mechanism and aid in developing high-performance photodynamic antibacterial metal NCs. In this study, our investigation focused on two main areas: (1) elucidating the valence band (VB)–conduction band (CB) transitions of the Arg-Au_{22} NCs to identify potential photodynamic reactions for ROS/RNS generation and (2) evaluating the specific contributions of various ROS/RNS species to bacterial eradication. To begin, the bandgap (E_g) and VB energy values of the Arg-Au_{22} NCs were established through VB-X-ray photoelectron spectroscopy (XPS) and UV-vis absorption measurements (Fig. S6 and S7†), yielding values of 2.15 eV for E_g, 2.22 V (*vs.* RHE) for the VB, and 0.07 V (*vs.* RHE) for the CB (Fig. 3a and

Published on 11 October 2024. Downloaded on 2/23/2026 2:18:25 PM.

ESI Note I†) calculated using the equation $E_g = E_{VB} - E_{CB}$.[28,31,33] Importantly, the potentials of $^{\bullet}OH$ were found to be 0.73 V (*vs.* RHE, pH = 7) and 1.96 V (*vs.* RHE, pH = 7), while that of H_2O_2 was found to be 0.28 V (*vs.* RHE, pH = 7). These values position them between the CB and VB potentials of the Arg-Au_{22} NCs, suggesting the thermodynamic feasibility of their generation. In comparison, the VB and CB potentials of pristine Au_{22} NCs were found to be 1.77 V and −0.37 V (Fig. 3a, Fig. S8, S9, and ESI Note I†), respectively. Notably, this VB–CB band encompasses the potential required for oxygen or H_2O_2 reduction ($O_2/^{\bullet}O_2^-$, −0.33 V *vs.* RHE, pH = 7; O_2/H_2O_2, 0.28 V *vs.* RHE, pH = 7; $H_2O_2/^{\bullet}OH$, 0.73 V *vs.* RHE, pH = 7), meeting the thermodynamic prerequisites for the production of $^{\bullet}O_2^-$ and H_2O_2 *via* O_2 reduction and the production of $^{\bullet}OH$ *via* H_2O_2 reduction. Therefore, it can be deduced that the Arg conjugation with the Au_{22} NCs may potentially transition the photodynamic ROS production modality, which would enhance the photodynamic antibacterial efficacy of the NCs.

To confirm the generation of ROS, electronic paramagnetic resonance (EPR) spectrometry and UV-vis absorption spectroscopy were utilized for both the Arg-Au_{22} NCs and pristine Au_{22} NCs (Fig. 3b–d and Fig. S10–S12†). Under visible light illumination, the EPR signal of $^{\bullet}OH$ was detected for the Arg-Au_{22} NCs (Fig. 3b), while no signals of $^{\bullet}O_2^-$ and singlet oxygen ($^1O_2$) were observed for the same sample under the same conditions (Fig. S10†). In contrast, the EPR signal of $^{\bullet}O_2^-$ was observed for pristine Au_{22} NCs under visible light illumination, with no signals of $^{\bullet}OH$ and $^1O_2$ detected for the same sample under the same conditions (Fig. S11†). Moreover, we also examined the H_2O_2 production capability of both the NCs based on a colorimetric assay using 2,9-dimethyl-1,10-phenanthroline (DMP) and cupric sulfate as indicators (see more details in section 1.6 in the ESI†). Upon 1 h of illumination, the absorbance of H_2O_2 at 454 nm markedly increased for the Arg-Au_{22} NCs, as evidenced by the data in Fig. 3c. This observation clearly indicates the pronounced photodynamic H_2O_2 generation capacity of the Arg-Au_{22} NCs, estimated to be approximately 1233 μM over the course of 1 h. In contrast, no H_2O_2 signal was detected for pristine Au_{22} NCs, as shown in Fig. S12.† Consequently, it can be concluded that the introduction of Arg conjugation to the Au_{22} NCs has a significant impact on the modality of photodynamic ROS production. This transformation is characterized by a shift from the sole production of $^{\bullet}O_2^-$ to the concurrent generation of H_2O_2 and $^{\bullet}OH$, endowing the NCs with enhanced oxidative destruction potential against bacteria and thus augmenting the photodynamic antibacterial performance of the Arg-Au_{22} NCs. Of note, the sole production of $^{\bullet}O_2^-$ rather than $^{\bullet}O_2^-$, $^{\bullet}OH$ and H_2O_2 (different from the depiction in Fig. 3a) by pristine Au_{22} NCs may be due to the similarity in energy levels between $^{\bullet}O_2^-$ production ($O_2/^{\bullet}O_2^-$, −0.33 V *vs.* RHE, pH = 7) and the CB of the Au_{22} NCs (−0.37 V), rendering $^{\bullet}O_2^-$ production more favorable.

In addition to altering the photodynamic ROS production modality, we surprisingly found that the Arg conjugation also endows the NCs with the capability of photodynamically producing RNS that are more toxic to bacteria.[35,42] As shown, the EPR signal of NO was observed for the Arg-Au_{22} NCs under visible light illumination (Fig. 3d), while an almost imperceptible signal of NO was detected for pristine Au_{22} NCs under the

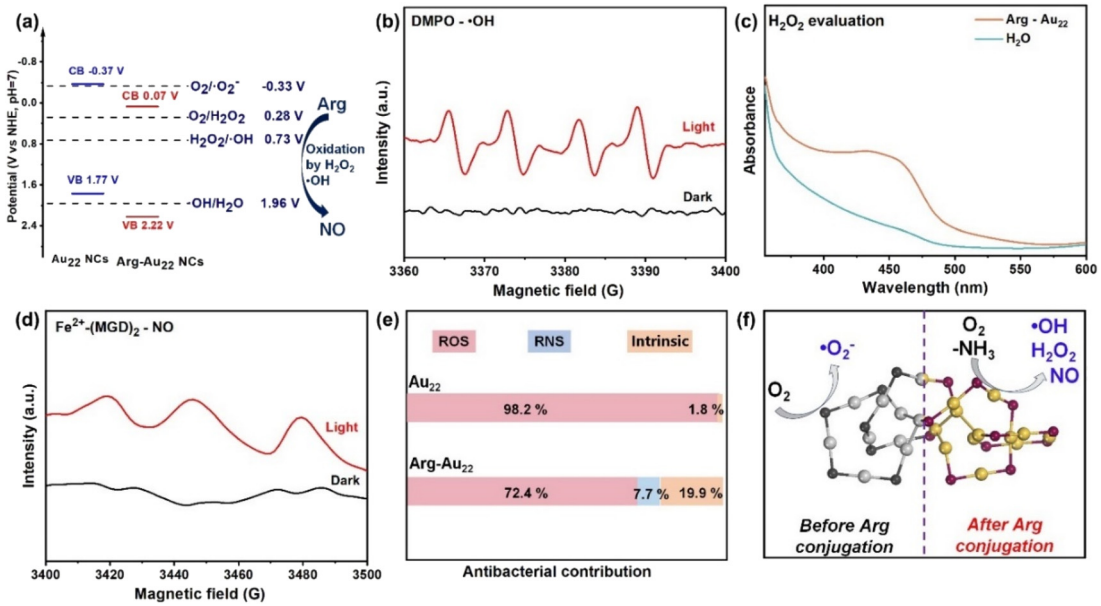

Fig. 3 (a) Energy level diagram of Arg-Au_{22} and pristine Au_{22} NCs. (b) EPR spectra of $^{\bullet}OH$ of the Arg-Au_{22} NCs with or without visible light illumination. (c) Absorbance of the generated H_2O_2 over Arg-Au_{22} NCs under visible light illumination and bubbling O_2 for 60 min. (d) EPR spectra of NO of the Arg-Au_{22} NCs with or without visible light illumination. (e) Specific antibacterial contributions of ROS, RNS and intrinsic antibacterial Au species over Arg-Au_{22} and pristine Au_{22} NCs. (f) Schematic illustration of the photodynamic ROS/RNS production modality of Au_{22} NCs before and after Arg conjugation.

 This journal is © The Royal Society of Chemistry 2024

Published on 11 October 2024. Downloaded on 2/23/2026 2:18:25 PM.

same conditions (Fig. S13†). Why does Arg conjugation endow Au_{22} NCs with excellent photodynamic RNS producibility? We have speculated that Arg conjugation renders Au_{22} NCs with exceptional photodynamic ROS production capability and it is the generation of abundant ROS that oxidizes the amino groups of Arg to NO with light irradiation, which has been supported by several reported studies involving photodynamic conversion of Arg to NO.[35,42]

To investigate the specific antibacterial contributions of the generated ROS, RNS, and intrinsic antibacterial activity of Arg-Au_{22} NCs, we conducted experiments aimed at elucidating this issue. Antibacterial tests were performed on Arg-Au_{22} NCs, pristine Au_{22} NCs, and PBS (as control) under various conditions, including darkness, visible light irradiation with O_2 bubbling in the presence of ROS scavengers (*e.g.*, 5,5-dimethyl-1-pyrroline *N*-oxide (DMPO)), and visible light irradiation with O_2 bubbling (Fig. S14† and Fig. 2). Through these experiments, the distinct contributions of ROS, RNS, and the intrinsic antibacterial activity of Au_{22} NCs could be discerned (ESI Note II†). As illustrated in Fig. 3e, in the case of Arg-Au_{22} NCs, the antibacterial efficacy was attributed to ROS (72.4%), RNS (7.7%) and intrinsic antibacterial Au species (19.9%). This contrasts significantly with the findings for pristine Au_{22} NCs, where ROS and intrinsic antibacterial Au species accounted for 98.2% and 1.8% of the antibacterial efficacy, respectively. The data collected also confirmed that the Arg conjugation on the surface of Au_{22} NCs led to modulation of the photodynamic ROS production modality, shifting from $^{\bullet}O_2^-$ to $^{\bullet}OH$ and H_2O_2, accompanied by extra RNS production (Fig. 3f). It should be emphasized that the Arg conjugation with Au_{22} NCs achieved a goal of "killing four birds with one stone", *i.e.*, Arg conjugation bolstered and enhanced the photodynamic production of ROS, stimulated the RNS production, enhanced the intrinsic antibacterial activity of Au NCs *via* surface-chemistry engineering, and improved the biocompatibility. In particular, the synergistic coupling of the photodynamic ROS/RNS production and the intrinsic antibacterial activity of Au NCs contributes to the exceptional antibacterial activity of the Arg-Au_{22} NCs. Overall, these findings may provide insightful clues on the design of novel metal NC-based photodynamic antibacterial agents with multiple antibacterial modalities.

3.4. *In vivo* wound healing assessment

Fig. 4a illustrates the comprehensive evaluation process of photodynamic therapy utilizing Arg-Au_{22} NCs on mice with *E. coli*-infected wounds. Monitoring wound-healing progression and examining haematoxylin- and eosin (H&E)-stained infected skin wound tissues revealed that the Arg-Au_{22} NCs with visible light exposure (Arg-Au_{22}-light group) demonstrated superior therapeutic performance for *E. coli*-infected wounds compared to other groups, including PBS, Au_{22} NCs under visible light illumination (Au_{22}-light group), Arg-Au_{22} NCs without visible light illumination (Arg-Au_{22} group), and even vancomycin (Van; the currently most effective advanced antibiotic for *E. coli* eradication). The analysis of wound imprinting and physiological changes in the mouse model regarding the infected wound area,[3] body weight, and healing rate further confirmed that the Arg-Au_{22}-light group outperformed the other groups (Fig. 4c–e). For instance, on day 11, the respective wound areas for the PBS group, the Van group, the Au_{22}-light group, the Arg-Au_{22} group, and the Arg-Au_{22}-light group were measured as 13.42 ± 0.23 mm^2, 11.17 ± 0.17 mm^2, 10.00 ± 0.15 mm^2, 7.00 ± 0.14 mm^2, and 6.50 ± 0.07 mm^2, respectively, illustrating the efficacy of the Arg-Au_{22}-light group in wound healing (Fig. 4c). Moreover, the Arg-Au_{22}-light group demonstrated a more potent therapeutic effect compared to the Arg-Au_{22} group, emphasizing the synergistic coupling of photodynamic ROS/RNS production and the intrinsic antibacterial activity of Au NCs in enhancing antibacterial activity. Importantly, the therapeutic groups containing Arg-Au_{22} NCs effectively suppressed wound infection and accelerated wound healing compared to the Van group, suggesting the promising potential of Arg-Au_{22} NC-based antibacterial agents for clinical applications (Fig. 4b–e).[48]

Skin remodeling and regeneration are vital aspects of wound treatment during the Arg-Au_{22} NC therapy process. Histopathological changes at the *E. coli*-infected wound site following treatment are evident as shown in Fig. 4b (right panel). The skin tissues of the PBS, light, and Au_{22}-light groups showed severe damage to epidermal and dermal structures, whereas the Arg-Au_{22} group, the Arg-Au_{22}-light group, and the Van group exhibited intact regenerated epithelial tissue with recovery to its normal histological state similar to that of the Un-inf group. These findings highlight the ability of Arg-Au_{22} NCs to effectively eradicate bacteria and enhance the healing of *E. coli*-infected skin wounds. The therapeutic efficacy of Arg-Au_{22} NCs can be attributed to their outstanding photodynamic antimicrobial activity and the anti-inflammatory properties of their Arg–GSH ligands. Evaluation of key inflammatory factors such as IL-6, IL-1β, and TNF-α post-antibacterial treatment in the animal experiment revealed significant anti-inflammatory effects in mice treated with Arg-Au_{22}-light and Van.[49] On day 11, the levels of inflammatory factors in these treatment groups approached those of the Un-inf group, indicating the successful eradication of *E. coli* infection without inflammatory stress. Overall, the Arg-Au_{22} NCs exhibited remarkable photodynamic performance in accelerating the healing of wounds caused by *E. coli* infection.

Following the treatment experiment, the mice were euthanized and dissected to evaluate the biocompatibility of Arg-Au_{22} NCs with their major organs, including the heart, liver, spleen, lungs, and kidneys. Histopathological examination of H&E staining in the major organs of mice treated with Arg-Au_{22}-light indicated no significant differences (Fig. 5a), suggesting that the Arg-Au_{22} NCs do not induce damage to the major organs. Subsequently, a thorough examination of the blood and liver functions of mice treated with Arg-Au_{22} NCs was carried out, as illustrated in Fig. 5b. The outcomes of routine blood tests demonstrated that the lymph count, hemoglobin count, and neutrophil count remained unaffected post-therapy with Arg-Au_{22} NCs, thereby confirming their safety profile and minimal toxicity. Furthermore, the liver function

Published on 11 October 2024. Downloaded on 2/23/2026 2:18:25 PM.

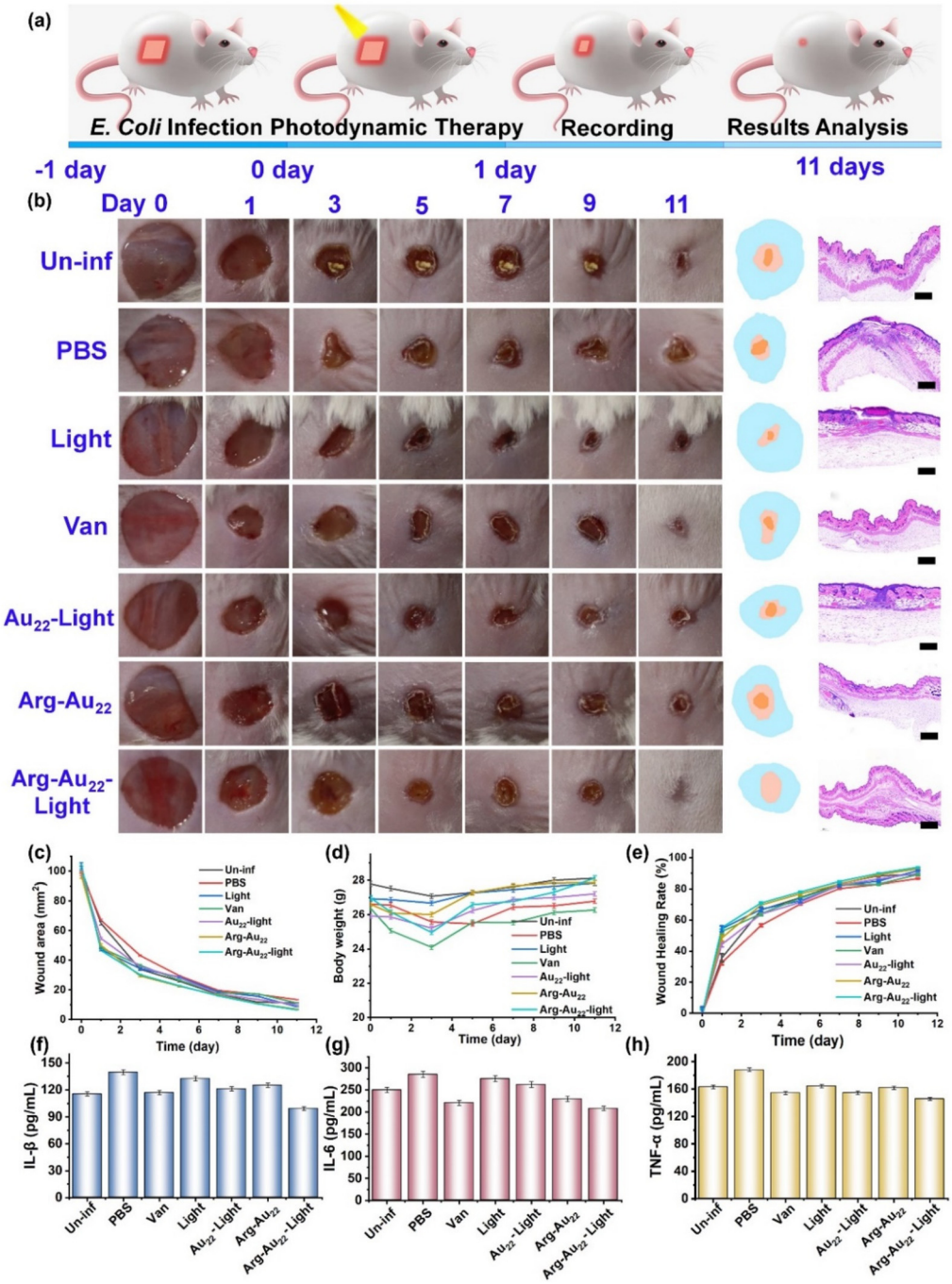

Fig. 4 Arg-Au_{22} NCs accelerating the healing of *E. coli*-infected skin wounds. (a) Schematic illustration of the animal experimentation timeline. (b) Digital images of wound change, wound imprinting analysis, and infected skin wound tissue evaluated by H&E staining in *E. coli*-infected mice after treatment with PBS, vancomycin (Van), Au_{22} NCs under visible light illumination for 5 min (Au_{22}-light group), and Arg-Au_{22} NCs with and without visible light illumination for 5 min within 11 days (scale bar: 500 μm). The Un-inf group represents uninfected skin wounds. (c) Wound area, (d) body weight change, and (e) wound healing rate in *E. coli*-infected mice from day 1 to day 11 during the treatment. Levels of (f) IL-1β, (g) IL-6, and (h) TNF-α in mice serum after the end of treatment.

test exhibited no notable variances between the treated mice and the reference. The measured levels of alanine aminotransferase, alkaline phosphatase, and albumin fell within the standard reference range, signifying that the liver function of the treated mice was essentially normal. In conclusion, these results collectively attest to the favorable biosafety profile of Arg-Au_{22} NCs when utilized in the management of *E. coli*-infected wounds.

 This journal is © The Royal Society of Chemistry 2024

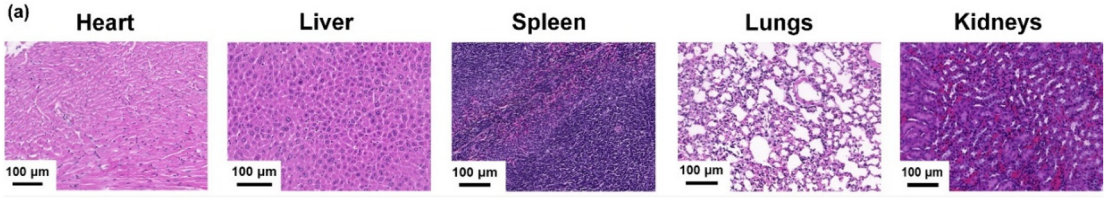

(b)

Name	Lymph (%)	Hemoglobin (g/L)	Neutrophil (10^9/L)	Alanine aminotransferase (U/L)	Alkaline phosphatase (U/L)	Total protein (g/L)	Albumin (g/L)
Acquired value	67.87	139	1.3	52.53	151.9	49.6	31.8
Normal range	55.8 – 90.6	110 - 143	0.1 - 1.8	28 - 132	62 - 209	36 - 66	25 - 48

Fig. 5 (a) H&E-stained histological imaging of the heart, liver, spleen, lungs, and kidneys (scale bar: 100 μm) in mice treated with Arg-Au_{22}-light. (b) Results of routine blood and liver function tests in wound-infected mice treated with Arg-Au_{22}-light.

Published on 11 October 2024. Downloaded on 2/23/2026 2:18:25 PM.

4. Conclusion

In summary, an ultrasmall Au NC-based photodynamic antibacterial agent has been designed to enhance the healing of bacteria-infected wounds by conjugating Arg molecules on the surface of AIE-featured Au_{22} NCs. The conjugation of Arg with Au_{22} NCs resulted in several beneficial effects, namely that effective modulation of the photodynamic ROS production modality, stimulated the RNS production, enhanced the intrinsic antibacterial activity of Au NCs, and improved biocompatibility. These enhancements enabled the Arg-Au_{22} NCs to combine ROS/RNS-mediated antibacterial action with the inherent antibacterial properties of Au NCs, leading to outstanding photodynamic antibacterial efficacy against broad-spectrum bacteria. *In vivo* experiments demonstrated the effective treatment of bacteria-infected wounds by Arg-Au_{22} NCs, resulting in the eradication of bacterial infections and reduced inflammation in the skin wound area. Importantly, Arg-Au_{22} NCs exhibited low cytotoxicity and high biosafety, as evidenced by the absence of organ damage and no adverse effects on blood biochemistry and liver functions. This study provides a paradigm in the design of Au NC-based photodynamic antibacterial agents with the modulation of photodynamic ROS/RNS production modalities for *in vivo* therapeutic applications, contributing to the understanding of ROS/RNS-mediated antibacterial mechanisms, and laying the groundwork for the future use of metal NCs in antibacterial therapies.

Ethics statement

This study was performed in strict accordance with the NIH guidelines for the care and use of laboratory animals (NIH Publication No. 85-23 Rev. 1985) and approved by both the Biomedical Ethics Committee of Universiti Malaysia Sabah and the Biomedical Ethics Committee of Qingdao Zhong Hao Biological Engineering Co., Ltd (Qingdao, China).

Data availability

The data that support the findings of this study are available from the corresponding authors (Xinyue Dou, Jianping Xie, and Coswald Stephen Sipaut) upon reasonable request.

The data supporting this article have been included as part of the ESI.†

Conflicts of interest

There are no conflicts to declare.

Acknowledgements

The authors acknowledge the Faculty of Engineering, Universiti Malaysia Sabah for its support and assistance in this research work. The authors acknowledge members of Prof. Coswald's group for their guidance and support in this project. The authors gratefully acknowledge the financial support from the Natural Science Foundation of Shandong Province (ZR2019YQ07, China) and the Ministry of Education, Singapore, Academic Research Fund (AcRF, Grant No. A-0009186-01-00 and A-8000054-01-00). The authors also acknowledge Qingdao Zhong Hao Biological Engineering Co., Ltd, for assistance with the animal experiments.

References

1 K. Zheng, M. I. Setyawati, D. T. Leong and J. Xie, *Coord. Chem. Rev.*, 2018, **357**, 1–17.
2 G. Yang, Z. Wang, F. Du, F. Jiang, X. Yuan and J. Y. Ying, *J. Am. Chem. Soc.*, 2023, **145**, 11879–11898.
3 F. Jiao, W. Zhao, W. Zhao, Y. Wang, Y. Deng, S. Chang, J. Sun, Q. Lou, L. Wang, C.-X. Shan, Y. Xiao and L. Dong, *BMEMat*, 2023, **1**, e12055.
4 L. Wang, Q. Hou, W. Zheng and X. Jiang, *ACS Nano*, 2021, **15**, 17885–17894.

Published on 11 October 2024. Downloaded on 2/23/2026 2:18:25 PM.

5 Z. Pang, N. Ren, Y. Wu, J. Qi, F. Hu, Y. Guo, Y. Xie, D. Zhou and X. Jiang, *Adv. Mater.*, 2023, **35**, 2303562.
6 S. Wang, Y. Wang, Y. Peng and X. Yang, *ACS Appl. Mater. Interfaces*, 2019, **11**, 8461–8469.
7 L. Luo, W. Huang, J. Zhang, Y. Yu and T. Sun, *ACS Appl. Nano Mater.*, 2024, **7**, 2529–2545.
8 H. Liu, Y. Li, S. Sun, Q. Xin, S. Liu, X. Mu, X. Yuan, K. Chen, H. Wang, K. Varga, W. Mi, J. Yang and X.-D. Zhang, *Nat. Commun.*, 2021, **12**, 114.
9 T. Jia, Y.-X. Li, X.-H. Ma, M.-M. Zhang, X.-Y. Dong, J. Ai and S.-Q. Zang, *Nat. Commun.*, 2023, **14**, 6877.
10 Y.-e. Shi, J. Ma, A. Feng, Z. Wang and A. L. Rogach, *Aggregate*, 2021, **2**, e112.
11 W. Q. Shi, L. Zeng, R. L. He, X. S. Han, Z. J. Guan, M. Zhou and Q. M. Wang, *Science*, 2024, **383**, 326–330.
12 J. Chen, P. Gu, G. Ran, Y. Zhang, M. Li, B. Chen, H. Lu, Y.-Z. Han, W. Zhang, Z. Tang, Q. Yan, R. Sun, X. Fu, G. Chen, Z. Shi, S. Wang, X. Liu, J. Li, L. Wang, Y. Zhu, J. Shen, B. Z. Tang and C. Fan, *Nat. Mater.*, 2024, **23**, 271–280.
13 W. Zhong, K. Liang, W. Liu and L. Shang, *Chem. Sci.*, 2023, **14**, 8823–8830.
14 X. Cai, G. Saranya, K. Shen, M. Chen, R. Si, W. Ding and Y. Zhu, *Angew. Chem., Int. Ed.*, 2019, **58**, 9964–9968.
15 Y. Du, H. Sheng, D. Astruc and M. Zhu, *Chem. Rev.*, 2020, **120**, 526–622.
16 X. Jiang, B. Du and J. Zheng, *Nat. Nanotechnol.*, 2019, **14**, 874–882.
17 Q. Yao, L. Liu, S. Malola, M. Ge, H. Xu, Z. Wu, T. Chen, Y. Cao, M. F. Matus, A. Pihlajamäki, Y. Han, H. Häkkinen and J. Xie, *Nat. Chem.*, 2023, **15**, 230–239.
18 M. R. Narouz, K. M. Osten, P. J. Unsworth, R. W. Y. Man, K. Salorinne, S. Takano, R. Tomihara, S. Kaappa, S. Malola, C.-T. Dinh, J. D. Padmos, K. Ayoo, P. J. Garrett, M. Nambo, J. H. Horton, E. H. Sargent, H. Häkkinen, T. Tsukuda and C. M. Crudden, *Nat. Chem.*, 2019, **11**, 419–425.
19 S.-S. Zhang, S. Havenridge, C. Zhang, Z. Wang, L. Feng, Z.-Y. Gao, C. M. Aikens, C.-H. Tung and D. Sun, *J. Am. Chem. Soc.*, 2022, **144**, 18305–18314.
20 D. Bera, A. Mukhopadhyay, Nonappa and N. Goswami, *J. Phys. Chem. Lett.*, 2023, **14**, 7299–7305.
21 X. Wang, B. Yin, L. Jiang, C. Yang, Y. Liu, G. Zou, S. Chen and M. Zhu, *Science*, 2023, **381**, 784–790.
22 X. Wang, Z. Wang, S. Fang, Y. Hou, X. Du, Y. Xie, Q. Xue, X. Zhou and X. Yuan, *Chem. Eng. J.*, 2021, **420**, 127589.
23 K. Zheng, M. I. Setyawati, D. T. Leong and J. Xie, *Chem. Mater.*, 2018, **30**, 2800–2808.
24 X. Zhang, Z. Zhang, Q. Shu, C. Xu, Q. Zheng, Z. Guo, C. Wang, Z. Hao, X. Liu, G. Wang, W. Yan, H. Chen and C. Lu, *Adv. Funct. Mater.*, 2021, **31**, 2008720.
25 J. C. Kuo, S. H. Tan, Y. C. Hsiao, C. Mutalik, H. M. Chen, S. Yougbaré and T. R. Kuo, *ACS Sustainable Chem. Eng.*, 2022, **10**, 464–471.
26 A. Luceri, R. Francese, S. Perero, D. Lembo, M. Ferraris and C. Balagna, *ACS Appl. Mater. Interfaces*, 2024, **16**, 3955–3965.
27 Z. Wei, T. Xu, C. Wang, S. Liu, W. Zhang, J. Sun, H. Yu, H. Shi and Y. Song, *Nanoscale*, 2024, **16**, 10656–10662.
28 H. Zhu, S. Wang, Y. Wang, C. Song, Q. Yao, X. Yuan and J. Xie, *Biomaterials*, 2022, **288**, 121695.
29 H. Wang, Q. Li, P. Alam, H. Bai, V. Bhalla, M. R. Bryce, M. Cao, C. Chen, S. Chen, X. Chen, Y. Chen, Z. Chen, D. Dang, D. Ding, S. Ding, Y. Duo, M. Gao, W. He, X. He, X. Hong, Y. Hong, J.-J. Hu, R. Hu, X. Huang, T. D. James, X. Jiang, G.-i. Konishi, R. T. K. Kwok, J. W. Y. Lam, C. Li, H. Li, K. Li, N. Li, W.-J. Li, Y. Li, X.-J. Liang, Y. Liang, B. Liu, G. Liu, X. Liu, X. Lou, X.-Y. Lou, L. Luo, P. R. McGonigal, Z.-W. Mao, G. Niu, T. C. Owyong, A. Pucci, J. Qian, A. Qin, Z. Qiu, A. L. Rogach, B. Situ, K. Tanaka, Y. Tang, B. Wang, D. Wang, J. Wang, W. Wang, W.-X. Wang, W.-J. Wang, X. Wang, Y.-F. Wang, S. Wu, Y. Wu, Y. Xiong, R. Xu, C. Yan, S. Yan, H.-B. Yang, L.-L. Yang, M. Yang, Y.-W. Yang, J. Yoon, S.-Q. Zang, J. Zhang, P. Zhang, T. Zhang, X. Zhang, X. Zhang, N. Zhao, Z. Zhao, J. Zheng, L. Zheng, Z. Zheng, M.-Q. Zhu, W.-H. Zhu, H. Zou and B. Z. Tang, *ACS Nano*, 2023, **17**, 14347–14405.
30 Z. Zuo, X. Pan, G. Yang, Y. Zhang, X. Liu, J. Zha and X. Yuan, *Dalton Trans.*, 2023, **52**, 2942–2947.
31 N. Liu, Y. Wang, Z. Wang, Q. He, Y. Liu, X. Dou, Z. Yin, Y. Li, H. Zhu and X. Yuan, *Nanoscale*, 2022, **14**, 8183–8191.
32 Z. Liu, Z. Wu, Q. Yao, Y. Cao, O. J. H. Chai and J. Xie, *Nano Today*, 2021, **36**, 101053.
33 H. Zhu, N. Liu, Z. Wang, Q. Xue, Q. Wang, X. Wang, Y. Liu, Z. Yin and X. Yuan, *Nanoscale*, 2021, **13**, 18996–19003.
34 Y. Wang, Y. Yang, Y. Shi, H. Song and C. Yu, *Adv. Mater.*, 2020, **32**, 1904106.
35 Y. Chen, X. Shu, J. Y. Guo, Y. Xiang, S. Y. Liang, J. M. Lai, J. Y. Zhou, L. H. Liu and P. Wang, *J. Controlled Release*, 2024, **367**, 248–264.
36 K. Yi, Y. Yu, L. Fan, L. Wang, Y. Wang and Y. Zhao, *Aggregate*, 2024, **5**, e509.
37 T. Richards, J. H. Harrhy, R. J. Lewis, A. G. R. Howe, G. M. Suldecki, A. Folli, D. J. Morgan, T. E. Davies, E. J. Loveridge, D. A. Crole, J. K. Edwards, P. Gaskin, C. J. Kiely, Q. He, D. M. Murphy, J.-Y. Maillard, S. J. Freakley and G. J. Hutchings, *Nat. Catal.*, 2021, **4**, 575–585.
38 Y. Yu, Z. Luo, D. M. Chevrier, D. T. Leong, P. Zhang, D.-e. Jiang and J. Xie, *J. Am. Chem. Soc.*, 2014, **136**, 1246–1249.
39 Z. Wang, X. Pan, S. Qian, G. Yang, F. Du and X. Yuan, *Coord. Chem. Rev.*, 2021, **438**, 213900.
40 B. Zhang, C. Chen, W. Chuang, S. Chen and P. Yang, *J. Am. Chem. Soc.*, 2020, **142**, 11514–11520.
41 S. Qian, Z. Wang, Z. Zuo, X. Wang, Q. Wang and X. Yuan, *Coord. Chem. Rev.*, 2022, **451**, 214268.
42 J. J. Wang, T. He, L. Chen, G. Xu, S. Dong, Y. Zhao, H. Zheng, Y. Liu and Q. Zeng, *Int. J. Food Microbiol.*, 2024, **411**, 110539.
43 D. Bera and N. Goswami, *J. Phys. Chem. Lett.*, 2021, **12**, 9033–9046.

 This journal is © The Royal Society of Chemistry 2024

44 D. Bera, M. Baruah, A. K. Dehury, A. Samanta, Y. S. Chaudhary and N. Goswami, *J. Phys. Chem. Lett.*, 2022, **13**, 9411–9421.
45 N. Goswami, Q. Yao, Z. Luo, J. Li, T. Chen and J. Xie, *J. Phys. Chem. Lett.*, 2016, **7**, 962–975.
46 H. Zhu, X. Yuan, Q. Yao and J. Xie, *Nano Energy*, 2021, **88**, 106306.
47 Y. Wang, Z. Zuo, Z. Wang, Y. Wu, J. Linghu, Y. Liu, H. Zhu, X. Dou, T. Feng and X. Yuan, *Chem. Eng. J.*, 2024, **492**, 152216.
48 S. Wang, W.-Y. Wu, J. C. C. Yeo, X. Y. D. Soo, W. Thitsartarn, S. Liu, B. H. Tan, A. Suwardi, Z. Li, Q. Zhu and X. J. Loh, *BMEMat*, 2023, **1**, e12021.
49 G. Yang, K. Liu, Y. Wang, X. Pan, J. Ye, Y. Li, F. Du, T. Feng and X. Yuan, *Aggregate*, 2024, **5**, e435.

Published on 11 October 2024. Downloaded on 2/23/2026 2:18:25 PM.